ISSN 1063-7710, Acoustical Physics, 2009, Vol. 55, No. 6, pp. 776–784. © Pleiades Publishing, Ltd., 2009.

OCEAN ACOUSTICS. HYDROACOUSTICS

Acoustic Manifestations of Gas Hydrate Shelled Bubbles

A. O. Maksimov and E. V. Sosedko

Il'ichev Pacific Oceanological Institute, Far-East Branch, Russian Academy of Sciences, ul. Baltiĭskaya 43, Vladivostok, 690041 Russia

e-mail: maksimov@poi.dvo.ru

Received June 18, 2008

Abstract—The hydrocarbon seeps emitting buoyant bubble plumes from seafloor vents—gas flares have been actively investigated in different regions of the World Ocean, in particular, on the Sakhalin slope in the Sea of Okhotsk. The gas flares can be easily detected by regular echo sounders, because the scattering cross section of a gas bubble is large. Within the gas-hydrate stability zone—for high hydrostatic pressures and low temperatures, methane-hydrate ice skins are formed on rising seep bubbles which are typically methane. The objective of the present study was to develop a suitable model describing rheological characteristics of gas-hydrate shell and to analyze acoustic manifestations of such bubbles for the frequency range used in marine field experiments.

PACS numbers: 43.30.+m, 92.10.Vz

DOI: 10.1134/S1063771009060128

INTRODUCTION

During the last decade, gas flares—bubble plumes of methane (CH_4) rising from the seabed into the water column were detected and actively investigated on the Sakhalin slope in the Sea of Okhotsk [1–5].

The persistence of methane gas bubble plumes in the ocean rising as much as hundreds meters in the water column is remarkable because the ocean is under-saturated in methane, and the bubbles should quickly dissolve. A probable explanation was proposed by Merewether et al. [6] who inferred that the bubbles were protected by a coating of oil or gas hydrate. The latter was suggested to cause the reduced shrinking rate of methane gas bubbles. Gas hydrate is an ice-like solid that results from the trapping of methane molecules—the main component of natural gas—within a lattice-like cage of water molecules. Gas clathrates (conventionally named gas hydrates) are crystalline solids, in which small non polar molecules (in this case—methane molecules) are trapped within a lattice-like cage of water molecules. The regimes of a hydrate skin formation on methane bubbles and dynamics of dissolution of such encapsulated bubbles have been the subjects of laboratory [7], as well as field [8] experiments.

Different types of echosounding systems were used during the experiments on the Sakhalin slope in the Sea of Okhotsk. However, most of the acoustic data were obtained for the systems operated at the frequencies of 12 and 19.7 kHz. Sonar proved to be of use for imaging these bubble plumes in the water column, and aided in locating and sampling of vent sites. Acoustic techniques allow the efficient location of the upper boundary of gas flares.

The dissolution rate of rising bubbles is controlled by partial pressure difference, sea water concentration of the dissolved gas, bubble size, and rise velocity. The formation of hydrate shells on gas bubbles [9, 10] can relate the observed difference in the vertical sizes of the acoustic plumes and the upper limit of the gas-hydrate stability zone (GHSZ). The gas hydrate skin will dissolve soon after the bubble rise above the stability zone and the subsequent methane flux from the bubble into the surrounding seawater increases considerably.

Figure 1 shows an example of the comparison of the height of the acoustic backscatter image of the gas flare at the frequency of 12 kHz and the upper boundary of the gas hydrate stability zone. The position the upper boundary of the stability zone has been evaluated on the basis of the method proposed in [9] for pure methane gas using the temperature profile taken at the seep site [3]. Acoustical observations have been made by Salomatin [4, 5] and we express him our gratitude for the possibility to use the echogram in our study. From this figure, it follows that there are correlations between the vertical size of the GHSZ and the height of gas flare determined on the base of the acoustic backscattering image. At the same time, this issue requires more detail investigation. In order to find the solution of this problem, the behavior of the bubbles coated by hydrate skin should be determined. In particular, one should analyze the peculiarities of their interaction with acoustical pulses transmitted by sonar. The preliminary results of this study have been presented at the RAS session [11].

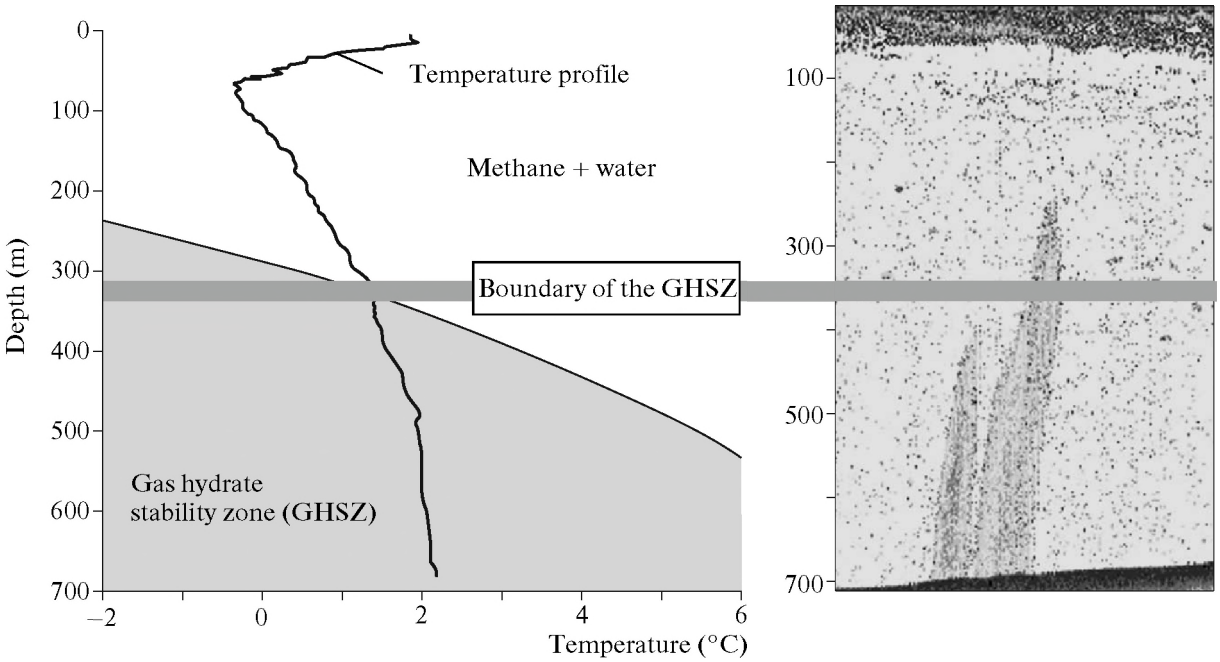

Fig. 1. Relationship between the height of the acoustic backscatter images and the upper boundary of the gas hydrate stability zone for the Obzhirov seepage.

The purpose of the present study was to develop a suitable model describing rheological properties of the hydrate shell. Such a model should be applicable for a wide range of various shell structures which include both a thin layer of ice and essentially more thick snow or pancake layer. A solution to the problem of acoustical pulse scattering from such encapsulated bubble should reveal prominent features on which basis it would be possible to make the conclusion regarding the presence (or absence) of the hydrate shell on the rising bubble. Along with the conventional (active) methods of bubble detection within the plume, the development of passive methods of analysis is of a definite interest. To characterize acoustic emission of oceanic bubbles, very picturesque expressions are used: "their birthing wails" [12], "seep bubble music" [13], etc. Thus, to find out the characteristic features of bubble emission attributed to the presence of the hydrate shell was also an objective of the present study.

SCATTERING FROM THE BUBBLE IN CONSOLIDATED SHELL

In order to analyze acoustic scattering from encapsulated bubble, we will use a clear similarity between acoustic manifestations of the hydrate shelled bubble and ultrasound contrast agent—microbubble whose surface is occupied by lipid or polymer molecules forming a shell and whose scattering signature provide a method of enhancing effectiveness of medical ultrasonic diagnostic [14–19]. The approximations based on the smallness of the bubble size R in comparison with the wavelength λ of the probing acoustical pulse are traditionally used in all works devoted to the problem of ultrasound scattering from contrast agents. The approximation of the incompressible shell being satisfied for the rubber like media, where sound speeds of the longitudinal and transversal waves are markedly different and where it is assumed that $R \ll \lambda$. However, for the rheological characteristics of the hydrate shells, the elastic modulus of which are very close to ones of the common ice and the modulus of shear μ coincides on the order of magnitude with the bulk modulus K, the approximation of incompressible shell is inapplicable.

In fact, for the given condition $R \ll \lambda$, the behavior of the shell is described by the quasi-static equilibrium equation—the biharmonic equation [20]:

$$\Delta\Delta\mathbf{u} = 0, \tag{1}$$

where $\mathbf{u}$—is the displacement of the shell element during deformation. Since the problem assumes spherical symmetry, the displacement vector is directed everywhere along the radius and depends upon the radial coordinate r only. Therefore $[\nabla \times \mathbf{u}] = 0$, and Eq. (1) reduces to $\nabla \mathrm{div}\mathbf{u} = 0$. Its solution has the form

$$\mathrm{div}\mathbf{u} = \frac{1}{r^2}\frac{d(r^2 u_r)}{dr} = \mathrm{const} \equiv 3a, \qquad u_r = ar + \frac{b}{r^2}, \tag{2}$$

where a and b are constants to be determined from boundary conditions. It is justified to neglect deformations leading to compressibility of the shell material—the

term containing the multiplier a, only in special cases, for example, for the rubber like media. On this reason, even though following the approach proposed in the papers [14–19], we need to present the details of calculation accounting for the corrections arising at $\mu/K \sim 1$.

The linear problem of scattering of plane sound wave $P(\mathbf{r}, t) = p_m \cos(kz - \omega t)$ (here ω is the frequency, $k = \omega/c_L$ is the wave vector, c_L is the sound speed in liquid, and p_m is the amplitude of the wave) from a bubble of radius R coated by visco-elastic shell of thickness h has an exact, but very cumbersome solution [21]. On this reason, we should use ad initial a number of approximations adherent to the problem. Based on currently available optical and acoustical data on the distribution of bubble sizes generated by marine seeps [13, 22], a crude model for this distribution can be used. It has a bell-like shape and is centered at $R \sim 2.5$ mm in the space of sizes. In the same time, the working frequencies of ship-board and research echosounding systems used for imaging these gas flares are in the frequency range from 3.5 till hundreds kHz. Thus, the wave length of imaging signals in water is always greater then bubble sizes. Moreover, the consideration of far-field (scattering amplitude) data is of interest. Therefore, we can take into account only the monopole component and neglect the contributions of higher multipoles. The solutions of the Helmholtz equation in liquid (L) and gas (G), and equations of the elastodynamics in shell (S) can be written in the form

$$
\begin{aligned}
P_L &= p_m \sum_{n=0}^{\infty} (2n+1) i^n [j_n(k_L r) + a_n h_n^{(1)}(k_L r)] P_n(\cos\vartheta) \\
&\approx p_m [j_0(k_L r) + a_0 h_0^{(1)}(k_L r)] \\
&\approx p_m \left[1 - \frac{(k_L r)^2}{3!} + a_0 \left(-\frac{i}{k_L r} + 1 \right) \right], \\
P_G &= p_m \sum_{n=0}^{\infty} (2n+1) i^n d_n j_n(k_G r) P_n(\cos\vartheta) \\
&\approx p_m d_0 \left[1 - \frac{(k_G r)^2}{3!} \right], \\
\varphi &= \frac{p_m}{\rho_S \omega^2} \sum_{n=0}^{\infty} (2n+1) i^n \\
&\times [b_n j_n(k_l r) + c_n y_n(k_l r)] P_n(\cos\vartheta) \\
&\approx \frac{p_m}{\rho_S \omega^2} \left[b_0 \left(1 - \frac{(k_l r)^2}{3!} \right) + c_0 \left(\frac{1}{k_l r} - \frac{k_l r}{2!} \right) \right], \\
u_r^{G,L} &= \frac{1}{\rho_{G,L} \omega^2} \frac{\partial P_{G,L}}{\partial r}, \quad u_r^S = \frac{\partial \varphi}{\partial r}, \\
\sigma_{rr} &= -\left(K - \frac{2}{3}\mu \right) k_l^2 \varphi + 2\mu \frac{\partial^2 \varphi}{\partial r^2},
\end{aligned}
\tag{3}
$$

where $j_n(k_\beta r)$, $h_n^{(1)}(k_\beta r)$, $y_n(k_\beta r)$ are the spherical Bessel functions (here the index β takes values: L—for liquid, G—for gas, l—for the longitudinal wave numbers in the shell); $P_n(\cos\vartheta)$ are the Legendre polynomials; the spherical coordinates (r, ϑ, α) are used; $u_r^{G,L,S}$ and $\rho_{G,L,S}$ are the radial displacements and density of the media in the bubble, in the outer liquid and in the shell; σ_{rr} is the radial component of the stress tensor; K and μ are the modulus of compression and shear; $c_l^2 = (K + 4\mu/3)/\rho_S$ is the speed of longitudinal waves in the shell. Owing to the symmetry of the problem, the oscillation displacements are directed along the sphere's radius and have a single component $u_r^{G,L,S}$. Moreover, since vorticity vanishes in this case $[\nabla \times \mathbf{u}] = 0$, transverse oscillations are not excited in the shell.

The constants a_0, b_0, c_0, d_0 are determined from the conditions of continuity of the radial displacement and the stress at the interfaces between the shell and gas $r = R$, and the shell and liquid $r = R + h$. By performing direct calculations, the scattering amplitude from the bubble covered by hydrate shell $f_0 = -ia_0/k_L$ can be worked out in the following form

$$
\begin{aligned}
f_0 &= -R \frac{\omega^2}{\omega^2 - \Omega_0^2 (1 - ik_L R)}, \\
\Omega_0^2 &= \left(3\gamma P_0 + 12\mu \frac{h}{R} \frac{1}{1 + 4\mu/3K} \right) (\rho_L R^2)^{-1}.
\end{aligned}
\tag{4}
$$

In derivation of this Eq. (4), we assumed that the behavior of the gas core is polytropic $c_G^2 = \gamma P_{g0}/\rho_G$, where P_{g0} is the equilibrium gas pressure in the bubble, γ is the polytropic index. For given conditions, the inequality $h \ll R$ is fulfilled with a large stock, thus allowing one to neglect the inhomogeneties of deformations and stresses within the shell. Equation (4) is distinguished from those that are used for description of scattering from contrast agents [17] by co-factor $(1 + 4\mu/3K)$. For rubber like shells $\mu/K \ll 1$, and in this case Eq. (3) takes the usual form [19]. However, for the hydrate shells, the elastic modulus of which are very close to ones of the common ice ($K \approx 7.5 \times 10^9$ Pa, $\mu \approx 3.5 \times 10^9$ Pa), [23] the correction factor should be accounted.

In considering scattering from consolidated shell (4) we did not account dissipative effects in liquid, shell and gas. This approximation is justified, since the zone of stability for gas-hydrates is located at depths in hundreds meters and high hydrostatic pressure in tens atmospheres provides that the dominant mechanism of losses near the resonance ($|\omega - \Omega_0|/\Omega_0 \ll 1$), where they should only be accounted, is the radiation damp-

ing. This type of losses has been accounted in derivation of Eq. (4).

Another peculiarity, that distinguishes cardinally the behavior of the scattering amplitude (4) from one for the conditions of the laboratory experiments with contrast agents, is the high equilibrium pressure in the bubble, which is near hydrostatic $P_h(z) = P_h(0)(1 + z/H)$, ($P_h(0) \approx 10^5$ Pa, $H \approx 10$ m), large, and varies with the depth z.

Figure 2 illustrates the variation of the back-scattering cross-section

$$\sigma_S = 4\pi R^2 \Omega^4 [(1-\Omega^2)^2 + (\omega R/c_L)^2]^{-1}, \quad \Omega = \omega/\Omega_0 \tag{5}$$

with the driving frequency for the frequency range $f = \omega/2\pi$: 3.5–135 kHz used at the field experiments on the Sakhalin slope in the Sea of Okhotsk, and for the interval of bubble sizes R: 0.1–5 mm. The values of physical parameters required to calculate the cross section (5) were chosen as follows: the sound speed in water was set equal to $c_L = 1453$ m/s, the depth was taken to be $z = 500$ m, the shell has thickness $h = 2$ μm, the bulk modulus K and the shear modulus μ were taken to be $K = 7.5 \times 10^9$ Pa and $\mu = 3.5 \times 10^9$ Pa. The results presented above have been based on the values of the elastic modules measured at laboratory conditions for the pure mono-crystal samples which are very close to the values for common ice [23]. The thickness of the hydrate layer h is the parameter which value is not reliably known. According to the laboratory observations [8], the optical properties of the hydrate layer on the bubble are similar to that of aluminum powder with crystallites seems to be of the order of a few microns. The calculations have been carried out within the wide range of the thickness, but for illustration (Fig. 2), it has been chosen equal to $h = 2$ μm corresponding to experimental conditions [8]. As it follows from formula (5) and Fig. 2, the character of scattering from a bubble with size smaller than 1 mm is already affected by the presence of a thin hydrate shell (one order of magnitude smaller than thickness of human hair). The maximum scattering cross section, corresponding to the resonance condition $\Omega = \omega/\Omega_0 = 1$, does not follow the curve $fR = 3.26$ in a plane of parameters f (in kHz), R (in mm) as it occurs for a common bubble near the sea surface, but has the following asymptotic behavior in the range of the small sizes and high frequencies $fR^{3/2} = (12\mu h)^{1/2}\rho_L^{-1/2}(1 + 4\mu/3K)^{-1/2}$. Note, that the quality factor of the bubble ceases to depend on the depth, since the radiation damping is now determined by the difference in impedance characteristics of shell and liquid, which, unlike of gas, are very weakly varied with the hydrostatic pressure.

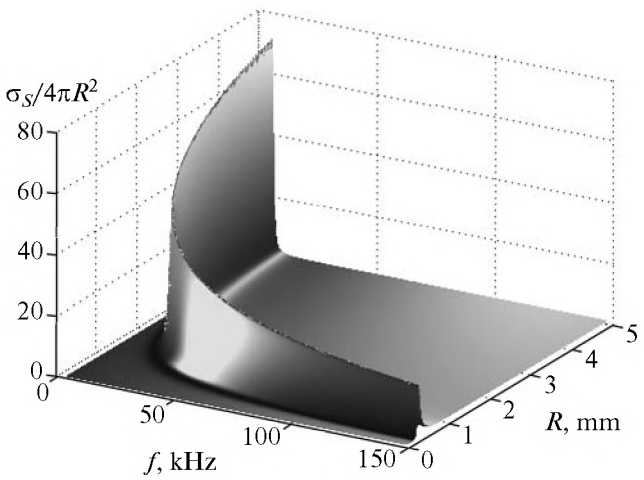

Fig. 2. The variation of scattering cross-section normalized on the bubble area ($\sigma_S/4\pi R^2$), with driving frequency $f = \omega/2\pi$ (in kHz) and bubble radius R (in mm) at the depth 500 m. The shell has thickness $h = 2.5$ μm and the shear modulus is equal to $\mu = 3.5$ GPa.

The gas-hydrate shell is formed in a few minutes [9] in natural conditions, however, within several seconds a seep bubble formed at the seabed will become covered by a layer of surface active substances. This means that the shell will contain a large number of impurities and defects, thus, as in the case of usual sea ice, the values of the elastic modulus can decrease on an order of magnitude $K \approx 6.5 \times 10^8$ Pa, $\mu \approx 3 \times 10^8$ Pa [23].

SHELL RUPTURE

In evaluating the scattering cross section (Fig. 2), we neglected the difference between hydrostatic pressure $P_h(z)$ and gas pressure in the bubble P_{g0}. This approach is justified at the stage not too far away in time from the moment when shell formation is finished. Decreasing of hydrostatic pressure acting upon a wall of the rising bubble will lead to the difference between internal P_g and external $P_h(z)$ pressures, therefore the condition of mechanical equilibrium for the shelled bubble requires an additional research.

Let at the depth z_0 the bubble is in equilibrium state: $P_{g0} = P_h(z_0)$. The internal and external radiuses of the shell are R_{10} and R_{20}, correspondingly. Note, that the shell is deformed at this state: $R_{20} - R_{2e} \approx R_{10} - R_{1e} = -R_{10}(P_h(z_0)/3K)$, where R_{2e} and R_{1e} are the equilibrium radii of the nondeformed shell [15, 19]. Parameters of the state at the depth z_1 ($(z_0 - z_1)/z_0 \ll 1$) are defined by an equilibrium condition within phases and a continuity of pressure and displacement on interface surfaces. According to [20], the stretching

stress in the shell at the depth z_1 will be defined by the expression (2), where

$$a = \frac{R_1^3 P_g - R_2^3 P_h(z_1)}{3K(R_2^3 - R_1^3)}, \quad b = \frac{(P_g - P_h(z_1))R_1^3 R_2^3}{4\mu(R_2^3 - R_1^3)},$$

$$P_g = P_{g0}\left(\frac{R_{10}}{R}\right)^{3\gamma} \approx P_h(z_0)\left(1 - 3\gamma\frac{R_1 - R_{10}}{R_{10}}\right),$$

$$u(R_1) = R_1 - R_{1e} = (R_1 - R_{10}) + (R_{10} - R_{1e}),$$

$$u(R_2) = R_2 - R_{20} = (R_2 - R_{20}) + (R_{20} - R_{2e}).$$

After introducing dimensionless variables

$$\xi \equiv (R_1 - R_{10})/R_{10}, \quad \eta \equiv (R_2 - R_{20})/R_{20},$$
$$\tau \equiv (R_{20} - R_{10})/R_{10},$$

which, under our assumption, are small parameters, and expanding deformations in a series in these variables to a first order accuracy, we obtain

$$\xi = \frac{[P_h(z_0) - P_h(z_1) - 3\gamma P_h(z_0)\xi]}{9K(\tau + \eta - \xi)}$$
$$+ \frac{[P_h(z_0) - P_h(z_1) - 3\gamma P_h(z_0)\xi]}{12\mu(\tau + \eta - \xi)} - \frac{(P_h(z_1) - P_h(z_0))}{3K},$$

$$\eta = \frac{[P_h(z_0) - P_h(z_1) - 3\gamma P_h(z_0)\xi]}{9K(\tau + \eta - \xi)}$$
$$+ \frac{[P_h(z_0) - P_h(z_1) - 3\gamma P_h(z_0)\xi]}{12\mu(\tau + \eta - \xi)} - \frac{(P_h(z_1) - P_h(z_0))}{3K}.$$

Whence it follows, that in the main order these variables are defined by the following equations

$$\eta = \xi, \quad \xi = \frac{[P_h(z_0) - P_h(z_1)]\left(1 + \frac{4\mu}{3K}\right)}{\left[12\mu\tau + 3\gamma P_h(z_0)\left(1 + \frac{4\mu}{3K}\right)\right]}.$$

The parameters a and b defining the stress and strain values within the shell at the horizon z_1 take the form

$$a(z_1) = \frac{1}{3K}\left\{-P_h(z_1) + \frac{4\mu[P_h(z_0) - P_h(z_1)]}{\left[12\mu\tau + 3\gamma P_h(z_0)\left(1 + \frac{4\mu}{3K}\right)\right]}\right\},$$

$$b(z_1) = \frac{[P_h(z_0) - P_h(z_1)]R_{10}^3}{\left[12\mu\tau + 3\gamma P_h(z_0)\left(1 + \frac{4\mu}{3K}\right)\right]}.$$

Tensile strength of ice is near 10^6 Pa. The stretching stress in the shell is defined by the following expression

$$\sigma_{\vartheta\vartheta} = \sigma_{\alpha\alpha} = 3Ka + \frac{2\mu b}{r^3} \approx -P_h(z_1)$$
$$+ \frac{6\mu[P_h(z_0) - P_h(z_1)]}{\left[12\mu\tau + 3\gamma P_h(z_0)\left(1 + \frac{4\mu}{3K}\right)\right]}.$$

Therefore, rising over the distance

$$(z_0 - z_1) \geq 2(z_0 + 11H)\left[\tau + \frac{3\gamma P_0}{12\mu}\frac{z_0 + H}{H}\left(1 + \frac{4\mu}{3K}\right)\right], \quad (6)$$

the shell will rupture. The values of physical parameters required to evaluate (6) were chosen as follows: $z_0 = 500$ m, $h = 2$ μm, $R_{10} = 2.5$ mm, $K \approx 6.5 \times 10^8$ Pa, and $\mu \approx 3 \times 10^8$ Pa (dirty ice) [24]. Substituting these into (6) yields $(z_0 - z_1) \approx 9$ m. Thus, during the main time on their way to the boundary of gas-hydrate stability zone, the shell represents pancake ice. Therefore, along with the model of the consolidated layer considered above, rheological properties of which are defined by Kelvin–Voigt model, there can be more appropriate to use the model of unconsolidated medium that is a layer of snow.

SNOW SHELL

The rheological properties of snow and ice (under nondestructive loading) are described in terms of the Burgers model [25–27]. This model involves a linear relation between stress (and its first derivatives with respect to time) and strain (together with its time derivatives). There are strong experimental evidences that this model applies only to the dissipation of the shear energy, i.e. the stress and strain tensors in the Burger model are the deviatoric tensors. It is assumed that there is no dissipation of the compression energy, i.e. the traces of stress and strain are related by a traditional way:

$$\sigma_{ii} = (K/3)u_{ii}, \quad (7)$$

by the bulk modulus K. When writing this formula (7), the usual convention of implicit summation over repeated indices has been adopted. The relationship between the deviatoric components of the stress and strain tensors $\sigma'_{ij} = \sigma_{ij} - (1/3)\delta_{ij}\sigma_{kk}$, $u'_{ij} = u_{ij} - (1/3)\delta_{ij}u_{kk}$ is used to determine the Burgers model

$$\ddot{\sigma}'_{ij} + \left(\frac{\mu_M}{\eta_M} + \frac{\mu_M}{\eta_K} + \frac{\mu_K}{\eta_K}\right)\dot{\sigma}'_{ij} + \frac{\mu_M\mu_K}{\eta_M\eta_K}\sigma'_{ij}$$
$$= 2\mu_M\ddot{u}'_{ij} + \frac{\mu_M\mu_K}{\eta_M\eta_K}\dot{u}'_{ij}, \quad (8)$$

where the dots denote first and second time derivatives. The parameters entering into this equation are shear modulus and viscosity μ_M, η_M for the Maxwell unit $\dot{\sigma}'_{ij} + (\mu_M/\eta_M)\sigma'_{ij} = 2\mu_M\dot{u}'_{ij}$ (which we used earlier to describe properties of the gas-hydrate shell [4], see also [14, 19]), and shear modulus and viscosity μ_K, η_K for the Kelvin–Voigt unit $\sigma'_{ij} = 2\mu_K u'_{ij} + 2\eta_K\dot{u}'_{ij}$. These are two limiting cases of the Burgers model. Thus, equation (8) represents the four-parametric approximation for estimation of rheological properties of snow.

For periodic external forcing $\sigma'_{ij}, u'_{ij} \sim e^{-i\omega t}$, calculations in the Burgers model (8) are reduced to

$$\begin{aligned} \sigma'_{ij}(\omega) &= 2\tilde{\mu}_M(\omega)u'_{ij}(\omega), \\ \sigma_{ij}(\omega) &= K\delta_{ij}u_{ll} + 2\tilde{\mu}_M(\omega)(u_{ij} - (1/3)\delta_{ij}u_{ll}), \\ \tilde{\mu}_M(\omega) &= \mu_M\frac{1 + i/(\omega\tau_K)}{1 + i[1/(\omega\tau_M) + (1 + \mu_M/\mu_K)/(\omega\tau_K)] - 1/(\omega\tau_K)(\omega\tau_M)}, \end{aligned} \tag{9}$$

where, for convenience, the relaxation times $\tau_M = \eta_M/\mu_M$, $\tau_K = \eta_K/\mu_K$, have been introduced.

The experimental determination of the parameters of the Burgers model is carried out under conditions which make it difficult to separate the contributions of purely shift and bulk deformations. On this reason, the results of measurements, as a rule, are Young's modulus and Poisson's ratio. The vast majority of the data refer to dry snow. Over the density range $\rho \sim 0.3$–$0.6\ \mathrm{g/sm^3}$, the real part of Young's modulus E_M obtained on the basis of measurements of propagation rate of acoustic impulses varies from 2×10^7 to 2×10^9 Pa with variation of Poisson's ratio σ from 0.2 to 0.3, correspondingly. The coefficient of viscosity η_M changes from 2×10^5 to 10^7 Pa over the same density range [25–27]. The elastic bulk modulus $K_M = E_M/3(1 - 2\sigma)$ and the shear modulus $\mu_M = E_M/2(1 + \sigma)$ may thus vary between the following limits: $1.1 \times 10^7 \le K \le 1.7 \times 10^9$ Pa, $8.3 \times 10^6 \le \mu \le 7.7 \times 10^8$ Pa.

The dependence of Young's modulus and coefficient of viscosity on snow microstructure: the character of the basic structural units, the geometrical arrangement of the structural units and the pore spaces, the nature of the bonds between the structural units is not so strong as its density dependence and corresponds to variation over a few times, instead of a few orders of magnitude [28, 29]. Bonds between ice crystallites and contact pressure, which is the main parameter characterizing bonds, decreased in wet snow. As a result, the ability of material to resist shear stress decreases, and the effective shear modulus can be of about one order magnitude smaller than the given values.

For the frequency range of interest in the current study 10–40 kHz, the Maxwell relaxation time $\tau_M = \eta_M/\mu_M$ considerably exceeds the period of oscillation $0.013 \le \tau_M \le 0.024$ s. It is therefore possible to neglect in the leading order the term $1/(\omega\tau_M)$ in formula (9) for the effective shear modulus. The Kelvin–Voigt relaxation time $\tau_K = \eta_K/\mu_K$ is significantly shorter. According to [26], its value lies within the interval $10^{-5} \le \tau_K \le 10^{-3}$ s and is of the same order of magnitude as the dielectric relaxation time in a single ice crystallite, thus in this case, $1/(\omega\tau_K) \le 1$, and for a rough estimate it is possible to put $\tilde{\mu}_M(\omega) = \mu_M$.

For a considered case of linear oscillations and for periodic external forcing, calculations in the Burgers model are reduced to the expression (4) provided the shear modulus μ_M is changed to renormalized one. Figure 3 illustrates the behavior of the scattering cross-section as a function of equilibrium radius and frequency. The values of other physical parameters were the same as used for calculation of Fig. 2 with two exceptions: the thickness of the shell was set equal to $h = 25$ μm and the shear modulus was taken equal to $\mu_M = 20$ MPa. This value μ_M corresponds to rigidity of not consolidated shell (wet snow). We did not account dissipative effects in the shell due to the smallness of its thickness and large depths where gas hydrates can only exist. In this case, the radiation damping of the bubble is the dominant loss mechanism. The rate of mass transfer is enhanced significantly in non-consolidated shell, since this process is not limited by a very slow diffusion of methane molecules to the external surface and water molecules to the internal surface of the gas hydrate shell. Accordingly, the thickness of the shell can be larger, therefore, for the estimation, we have chosen the value $h = 25$ μm.

Comparison of the scattering cross sections (Figs. 2 and 3) shows that the choice of the model of the shell is most important for the range of the small bubble sizes and to a lesser extent affects the character of scattering from larger bubbles for which the dominating factor is the compressibility of gas, instead of elasticity of shell. One should emphasize that presence of the shell affects the character of the scattering only for near resonant bubbles. For smaller bubbles the scattering follows to the Rayleigh law and they are irresolvable in the back scattering. The scattering cross section of greater bubbles is defined by their geometrical sizes.

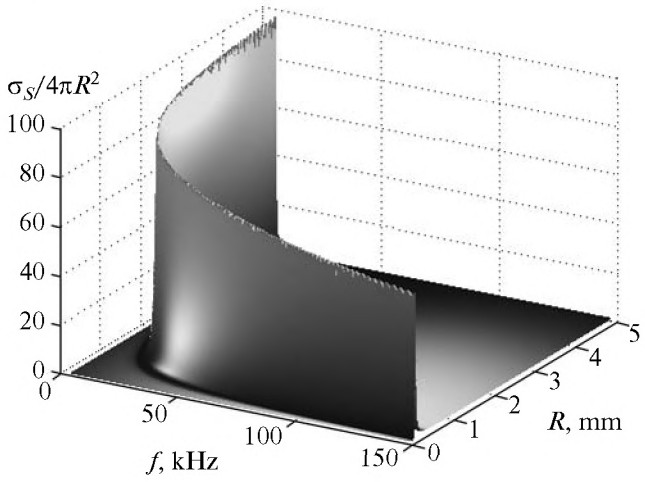

Fig. 3. The variation of scattering cross-section normalized on the bubble area ($\sigma_S/4\pi R^2$), with driving frequency $f = \omega/2\pi$ (in kHz) and bubble radius R (in mm) at the depth 500 m. The shell has thickness $h = 25$ μm and the shear modulus is equal to $\mu = 20$ MPa.

SOUNDS PRODUCED BY BUBBLES AT SHELL RUPTURE

Till now, we only considered the acoustic manifestations of the hydrate shelled bubbles by using active methods, which mean the transmitting and receiving the scattered signal. However, bubbles at the birth and during their rise to the surface can produce sounds by itself and, thus, allow to use the passive methods for diagnostics of gas flares. For the free bubbles (without shell), the noise spectrum emitted by marine hydrocarbon seeps was a subject both theoretical [30], and experimental studies [13]. The specific mechanism of acoustic emission attributed to the shelled bubble is realized at the moment of shell rupture. The subsequent radiation of the energy which was accumulated in the compressed (in comparison with external hydrostatic pressure) gas is accompanied by cavity pulsations. This mechanism is similar to one used in pneumatic seismic sources—air-gun [31] and is realized at underwater explosions [32].

The thin shell can sustain only some bars (some tens meters of rising) $(P_g(R) - P_h(z))/P_h(z) \ll 1$, therefore pulsations of the released cavity at the depth in hundreds meters will not be of a large amplitude. For the same reason the velocity of the bubble wall during the initial moment of shell rupture (after occurrence of cracks expanding over the shell) is essentially less than the sound speed in the surrounding liquid. As a result, we can neglect nonlinearity in the equations of state and conservation of mass for the liquid phase, and use the Rayleigh equation for the description of the dynamics of a cavity disengaged from the shell [32]

$$R\ddot{R} + \frac{3}{2}\dot{R}^2 = \frac{[p(R) - P_h(z)]}{\rho_L} + \frac{R\dot{p}(R)}{\rho_L c_L},$$

here $p(R)$ is the pressure on the liquid side of the cavity wall. One can not use the model of incompressible liquid in the derivation of the initial conditions to this equation. For this reason, the values of $\dot{R}(0)$ and $p(R_0, 0)$ are determined from the so-called p–u diagram [32].

After the shell has ruptured, a contact discontinuity is generated at the cavity interface where the pressure on the gas side of the interface is equal to $P_g(R_0)$ and that on the liquid side is $P_h(z)$. The contact discontinuity decays into the compression shock wave launched in the liquid and the rarefaction wave propagating in the opposite direction—in the gas. The pressures in the liquid before and behind the shock-wave front are $P_h(z)$ and p_2, respectively. The pressures in the gas before and behind the rarefaction front are $P_g(R_0)$ and p_2. We consider a short time interval after the discontinuity decay over which it is possible to neglect curvature of the interface and to analyze a one-dimensional problem. Liquid and gas flow rates at the interface coincide with the velocity of the moving interface u_2.

The presence of Riemann invariants for simple wave equations of one-dimensional motion allows to determine, on the base of the given equations of state for liquid and gas, the jumps of the particle velocity, density and pressure across the front of the shock wave in the liquid and the front of the rarefaction wave in the gas. The velocity of the contact discontinuity on the liquid side is given by [32]

$$u_2 \approx \frac{p_2 - P_h(z)}{\rho_L c_L}, \tag{10}$$

where we restricted analysis to the first order approximation in the Mach number. The velocity of the contact discontinuity on the gas phase side has a similar form

$$u_2 \approx \frac{P_g(R_0) - p_2}{\rho_G c_G}. \tag{11}$$

The continuity of pressure and particle velocity across the contact discontinuity after its decay, which leads to equality of the right hand sides of Eqs. (10) and (11), solves the initial conditions problem. Since the impedances of liquid $\rho_L c_L$ and gas $\rho_G c_G$ differ significantly, the initial pressure on the liquid side of the cavity $p(R_0, 0)$ and the velocity of the interface $\dot{R}(0)$ are given by the following simple expressions

$$\dot{R}(0) = u_2 \approx \frac{P_g(R_0) - P_h(z)}{\rho_L c_L}, \quad p(R_0, 0) \approx P_g(R_0).$$

For the difference between external and internal pressures in a few bars $(P_g(R_0) - P_h(z)) = (1–3) \times 10^5$ Pa leading to shell rupture, the initial velocity gained by

the bubble wall is $\dot{R}(0) \sim 7$–20 cm/s, which coincides in order of magnitude with the bubble rise velocity.

There are two circumstances: relatively low pressure $(P_g(R) - P_h(z))/P_h(z) \ll 1$ required to rupture the shell and small initial velocity of the bubble wall $\dot{R}(0) \ll R_0\Omega_0$, $[(P_g(R_0) - P_h(z))/\rho_L c_L] \ll \sqrt{3\gamma P_0/\rho_L}$, which enable us to describe the transition of the bubble from the initial into the final state (corresponding to the equilibrium bubble size at hydrostatic pressure $P_h(z)$) by use the linearized form of the Rayleigh equation.

$$\ddot{R} + \Omega_0^2 R = \left(\frac{P_h - P_0}{\rho_L R_0} + \frac{\dot{R}R_0\Omega_0^2}{c_L}\right). \quad (12)$$

The solution of Eq. (12) has the form

$$R = R_\infty + ae^{-\delta t}\cos(\Omega_0 t - \alpha),$$

$$R_\infty = R_0\left[1 + \frac{P_0 - P_h(z)}{3\gamma P_h(z)}\right], \quad a = R_0\frac{P_0 - P_h(z)}{3\gamma P_h(z)},$$

$$\alpha = \sqrt{\frac{3\gamma P_0}{\rho_L c_L^2}}, \quad \delta = R_0\Omega_0^2/2c_L.$$

The acoustic signal radiated by a bubble after destruction of the shell:

$$p(r, t) = \rho_L\frac{R_0^2\ddot{R}(t - r/c_L)}{r}$$
$$= -(P_0 - P_h(z))\frac{R_0}{r}\cos[\Omega_0(t - r/c_L) - \alpha]e^{-\delta(t - r/c_L)} \quad (13)$$

is much more intensive, than the sounds emitted from entrained bubbles (at the same depth d under the sea surface) after impacting of a rain drop (or sea splashes) a liquid surface. Bubbles entrained by rain impact will be near a water surface, which will cause the emission to take dipole form. The radiated pressure is given by [33]

$$p(r, \theta, t) = \left(\frac{2\sigma}{R_0} + \rho_L g d\right)\left(\frac{2d}{c_L}\cos\theta\right)\frac{R_0}{r}$$
$$\times \cos[\Omega_0(t - r/c_L)]e^{-\delta(t - r/c_L)},$$

where θ is the observation angle measured relative to the surface normal, σ is the surface tension coefficient, g is the acceleration of free fall, the depth of bubble formation h coincides in order of magnitude with its size.

The acoustic trace following bubble injection from a nozzle in laboratory studies (as a rule, at atmospheric pressure) has amplitude of orders magnitude smaller [33–35] than the radiation arising after destruction of the shell (13).

This effect—intense acoustic radiation accompanying shell fragmentation—can lead to the significant growth of noise level near a gas flare. The gas plume region represents an effective acoustic waveguide [30], which provides detection of this radiation against ambient ocean noise.

CONCLUSIONS

In the present study, definitive correlations have been established between the upper boundary of the gas hydrate stability zone and the heights of gas flares detected on the Sakhalin slope. This is an argument in favour of the formation of a gas-hydrate skin on rising methane bubbles. Several models for prediction of rheological behavior of gas hydrate shell have been proposed and analyzed in a wide range of characteristics: from clean ice to wet snow. The possibility to detect the presence of a shell on the bubble wall and to evaluate its parameters exists only if resonant scattering becomes dominant. It is shown that difference of hydrostatic pressure in some bars destroys the consolidated shell. Analytical expression for the shape of the acoustic signal radiated by a bubble after rupture of the shell has been derived. This radiation appears intensive enough, exceeding in orders of magnitude the noise of a rain or "birthing wails" of the bubbles as they depart from the vent.

ACKNOWLEDGMENTS

This work was supported by the Russian Foundation for Basic Research (project no. 08-05-000388).

REFERENCES

1. A. I. Obzhirov, B. A. Kazanskii, and Yu. I. Mel'nichenko, Tikhookean. Geol., No. 2, 119 (1989).
2. GEOMAR Report No. 82, Cruise Reports: KOMEX Y and YI RV. Professor Gagarinsky Cruise 26 and MV Marshal Gelovany Cruise 1, Ed. by N. Biebow (Kiel, 1999).
3. GEOMAR Report No. 110, Cruise Reports: KOMEX II and RV. Academic M. A. Lavrentyev, Cruise 29, Ed. by N. Biebow (Kiel, 2002).
4. A. S. Salomatin and V. I. Yusupov, in *Proc. of the 13th RAO Session* (GEOS, Moscow, 2003), Vol. 4, pp. 145–148.
5. A. S. Salomatin, V. I. Yusupov, and O. S. Otroshchenko, in *Proc. of the 10th Sci. School-Seminar of Acad. L.M. Brekhovskikh on Ocean Acoustics, and 14th RAO Session* (GEOS, Moscow, 2004), pp. 300-303.
6. R. Merewether, M. S. Olsson, and P. Lonsdale, J. Geophys. Res. B **90**, 3075 (1985).
7. Y. F. Makagon, *Hydrates of Hydrocarbons* (Penn Well, Tulsa, 1997).
8. N. A. Gumerov and G. Chahine, in *Proc. of the 8th Intern. Offshore and Polar Engin. Conf.* (Int. Soc. Offshore Polar Eng., Montreal, Canada, 1998), pp. 1–7.
9. G. Rehder et al., Geophys. Res. Lett. **29**, 1731 (2002).
10. K. U. Heeschen, A. M. Tre'hu, R. W. Collier, E. Suess, and G. Rehder, Geophys. Res. Lett. **30**, 1643 (2003).

11. A. O. Maksimov and E. V. Sosedko, in *Proc. of the 16th RAO Session* (GEOS, Moscow, 2005), Vol. 3, pp. 234–237.
12. M. S. Longuet-Higgins, in *Proc. of the Conf. on Natural Physical Sources of Underwater Sound* (Academic, Cambridge, 1990), pp. 1–33.
13. I. Leifer and D. Tang, J. Acoust. Soc. Am. **121**, EL35 (2007).
14. N. De Jong, L. Hoff, T. Skotland, and N. Bom, Ultrasonics **30**, 95 (1992).
15. C. C. Church, J. Acoust. Soc. Am. **97**, 1510 (1995).
16. V. N. Alekseev and S. A. Rybak, Akust. Zh. **45**, 603 (1999) [Acoust. Phys. **45**, 535 (1999)].
17. L. Hoff, P. C. Sontum, and J. M. Hovem, J. Acoust. Soc. Am. **107**, 2272 (2000).
18. P. Marmottant, M. van der Meer, M. Emmer, et al., J. Acoust. Soc. Am. **118**, 3499 (2005).
19. A. A. Doinikov and P. A. Dayton, J. Acoust. Soc. Am. **121**, 3331 (2007).
20. L. D. Landau and E. M. Lifshitz, *Course of Theoretical Physics,* Vol. 7: *Theory of Elasticity* (Nauka, Moscow, 1982; Pergamon Press, New York, 1986).
21. G. S. Gaunaurd and M. F. Werby, J. Acoust. Soc. Am. **90**, 2536 (1991).
22. I. Leifer and I. MacDonald, Earth Planet. Sci. Lett. **210**, 411 (2003).
23. H. Shimizu, T. Kumazaki, T. Kume, and S. Sasaki, Phys. Rev. B **65**, 212102 (2002).
24. T. Toyota et al., J. Oceanography **63**, 393 (2007).
25. M. A. Mellor, in *Proc. of the Intern. Symp. on Snow Mechanics, Grindelwald, Switzerland, 1–5 Apr. 1974* (Int. Assoc. Hydrologic. Sci., Geneva, 1975), Vol. 114, pp. 251–291.
26. R. L. Hook, M. Mellor, W. F. Budd, et al., Cold Regions Sci. Technol. **3**, 263 (1980).
27. L. H. Shapiro et al., *Cold Regions Research Engin. Lab. Report, 97-3* (NH, Hanover, 1997).
28. K. C. Agrawal and R. K. Mittal, Defence Sci. J. **5**, 93 (1995).
29. C. Chandel, P. K. Srivastava, and A. Upadhyay, Defence Sci. J. **57**, 393 (2007).
30. A. O. Maksimov, Akust. Zh. **51**, 435 (2005) [Acoust. Phys. **51**, 511 (2005)].
31. M. H. Safar, Geophys. Prospect. **24**, 756 (1976).
32. V. K. Kedrinskii, *Hydrodynamics of Explosion: Experiment and Models* (SO RAN, Novosibirsk, 2000; Springer, Berlin, 2005).
33. T. Leighton, *The Acoustic Bubble* (Academic, London, 1994).
34. T. G. Leighton and A. J. Walton, Eur. J. Phys. **8**, 98 (1987).
35. R. Manasseh, A. Nikolovska, A. Ooi, and S. Yoshida, J. Sound Vibrat. **278**, 807 (2004).